Identification and properties of the ^1L_a and ^1L_b states of pyranine

D. B. Spry, A. Goun, C. B. Bell III, and M. D. Fayer[a)]
Department of Chemistry, Stanford University, Stanford, California 94305

(Received 8 August 2006; accepted 7 September 2006; published online 11 October 2006)

The spectroscopic locations of the ^1L_a and ^1L_b electronic states of pyranine (1-hydroxy-3,6,8-pyrenetrisulfonic acid, commonly referred to as HPTS), as well as several related compounds, are found using magnetic circular dichroism spectroscopy as well as absorption and fluorescence spectroscopies. These electronic states have been discussed in connection with the photoacid properties of HPTS. Polarization selective fluorescence spectroscopy is used to identify the transition dipole directions of the electronic states of the compounds studied. The issue of the origin for the changes in vibronic structure of HPTS in different solvents is addressed. It is demonstrated that a Brownian oscillator model, in which the strength of the coupling of the electronic states to the solvent changes with solvent, is sufficient to reproduce the trends in the shapes of the vibronic structure. © *2006 American Institute of Physics*. [DOI: 10.1063/1.2358685]

I. INTRODUCTION

1-hydroxy-3,6,8-pyrenetrisulfonic acid, commonly referred to as HPTS or pyranine, has been one of the most useful molecules for studying excited state proton transfer in solution. First studied by Förster[1] and Weller[2] in the 1950s, HPTS has long interested scientists for its dramatic change in *pKa* upon photoexcitation. The change in *pKa* results in the release of a proton in aqueous solution. HPTS has nearly unparalleled recombination kinetics in an aqueous environment, nearly twice as fast as the self-neutralization of water.[3] Huppert[4] and Pines *et al.*[5] investigated geminate recombination kinetics in an excited state proton transfer with HPTS. In the past decade, HPTS has received considerable attention for its behavior at short times. Understanding the short time (femtosecond and picosecond) dynamics of HPTS has the potential to provide information about the early steps in proton transfer processes.[6–8] There have been various interpretations of the short time dynamics for HPTS, including an inversion of electronic states,[9,10] ultrafast proton transfer,[11,12] and hydrogen bond reorganization.[13] However, because relatively little is known about the lowest lying electronic states of HPTS, it is difficult to evaluate the validity of such models. Even the precise positions of these states are not known for certain.

Furthermore, HPTS has a number of properties that have made it useful for studies in a variety of research areas. Its *pKa* is 7.7, which is conveniently near the *p*H of neutral water. The absorbance and fluorescence spectra of the protonated and deprotonated forms are well separated. It has a strong absorption and a large fluorescence quantum yield. In addition, HPTS is commercially available, stabile, and highly soluble in water and other solvents. Therefore, it is also one of the most popular chromophores for probing various properties of aqueous environments. Because of HPTS's widespread use for fundamental research in proton transfer reactions, as a general probe for polar solvents, and for various applications in industry, understanding the electronic states that are responsible for its properties is worthwhile.

In the past decade there have been several studies of the solvent dependence of the absorption and fluorescence spectra of HPTS.[14,15] Attempts to characterize the lowest excited electronic states have been made through solvatochromism studies and electronic structure calculations. Magnetic circular dichroism (MCD) spectroscopy differs in these approaches in that it permits direct observations of electronic states even if they are overlapping. Here we use MCD to study the electronic states of HPTS and related compounds. In addition, the polarized fluorescence excitation spectra are used to assign the relative directions of the transition dipole moments of the states. HPTS and related molecules show substantial changes in the shape of the fluorescence band when the solvent is changed. Depending on the solvent, the fluorescence can display a significant vibronic structure or appear essentially featureless. It is demonstrated that a Brownian oscillator model, in which the strength of the coupling of the electronic states to the solvent changes with solvent, is sufficient to reproduce the trends in the shapes of the vibronic structure. It shown that the key feature for coupling HPTS to the solvent dynamics is the ability of the solvent to donate a hydrogen bond.

II. EXPERIMENTAL PROCEDURES

Pyrene, 1-hydroxypyrene (pyrenol), 8-hydroxypyrene-1,3,6-trisulfonic acid trisodium salt (HPTS), 8-methoxypyrene-1,3,6-trisulfonic acid trisodium salt (MPTS), 8-aminopyrene-1,3,6-trisulfonic acid trisodium salt (APTS), and pyrene-1,3,6,8-tetrasulfonic acid tetrasodium salt [$Py(SO_3)_4$] were purchased from Aldrich and used as received (see Fig. 1). Spectroscopic grade hexane and glycerol were purchased from Fluka, and DMSO, methanol, formamide, *N*,*N*-dimethylformamide, and acetonitrile were acquired from Acros, Inc.

Ultraviolet-visible absorption spectra were measured on a Cary-6000i spectrophotometer. Fluorescence and aniso-

[a)]Electronic mail: fayer@stanford.edu

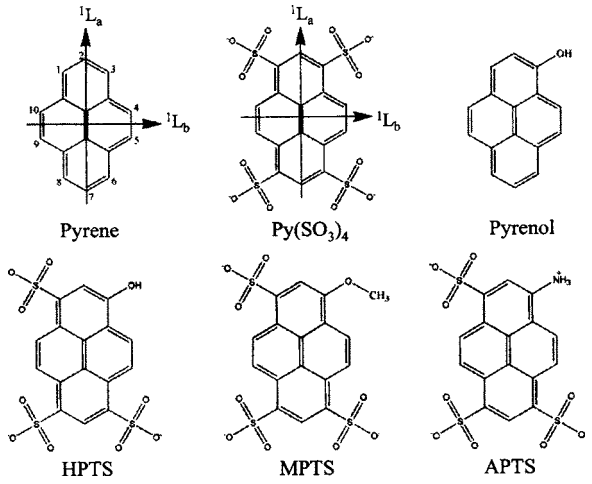

FIG. 1. Structure and abbreviations for molecules referred to in this paper.

tropy spectra were taken on a Fluorolog-3 fluorescence spectrometer. The fluorescence measurements were made at low concentration to avoid spectral distortion from emission reabsorption. The spectra were corrected for the Xe lamp intensity profile, monochromator, and photomultiplier response. A Janis VPF-100 cryostat was used for low temperature anisotropy measurements.

The MCD spectra were obtained using a Jasco 810 spectropolarimeter with S1 and S20 photomultiplier tubes as detectors and equipped with an Oxford Instruments SM4-7T superconducting magnet/cryostat. Samples were prepared in 100% glycerol with $\sim 10^{-4}M$ concentration and kept at 10 °C during data acquisition. The MCD spectra at both positive and negative fields were corrected for zero-field base line effects by subtracting off the corresponding 0 T scans. All spectra shown are measured at 7 T.

III. RESULTS AND DISCUSSION

A. Assigning the electronic states: Absorption, MCD, and polarization spectroscopy

To help understand the absorption and fluorescence spectra for HPTS, the closely related molecule pyrene-1,3,6,8-tetrasulfonic acid, which will be referred to as $Py(SO_3)_4$ (see Fig. 1) can provide valuable information because it differs only by one substituent, and it is more symmetric. The higher symmetry simplifies the absorption spectrum and forces the transition dipoles to align with either the long (a) or short (b) axis of the molecule, as illustrated in Fig. 1.

The absorption and fluorescence spectra along with the excitation and emission anisotropy of $Py(SO_3)_4$ in glycerol are shown in Fig. 2. The absorption spectrum shows three distinct transitions, all of which have a well-defined vibronic progression with a relatively constant spacing. Using the notation of Platt,[16] the three absorption bands are transitions to the ^1L_a, ^1B_b, and ^1B_a states. Due to the excellent mirror symmetry between the absorbance of the ^1L_a band and fluorescence line shape, the relatively short excited state lifetime, and the high fluorescence quantum yield, it can be concluded that fluorescence occurs from the strongly allowed ^1L_a transition.

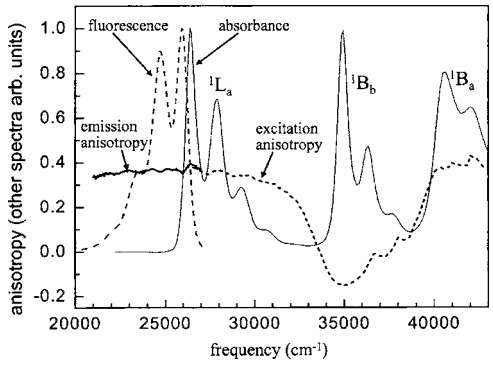

FIG. 2. Absorption, fluorescence, excitation anisotropy, and emission anisotropy spectra of $Py(SO_3)_4$ in glycerol. The anisotropy was measured at 77 K.

The excitation anisotropy spectrum (Fig. 2, dashed curve) shows the orientation of the absorption transition dipole relative to the fluorescing transition dipole. If the molecule is held in a rigid environment, such that reorientation time is much longer than the excited state lifetime, the anisotropy can be used to determine the relative directions of different transition dipoles in the molecule. All anisotropy spectra shown in this paper were taken at 77 K in pure glycerol glass. Under these conditions, no reorientation will occur. However, due to the relatively short excited state lifetime of the chromophores used and the high viscosity of glycerol at room temperature, the results are virtually identical to measurements that were made at room temperature. The degree of anisotropy is defined as

$$P = \frac{I_{\parallel} - I_{\perp}}{I_{\parallel} + 2I_{\perp}}, \tag{1}$$

where $I_{\parallel}$ and $I_{\perp}$ are the intensities of the components of emitted light parallel and perpendicular to the polarization of the excitation source, respectively. Because the molecule cannot rotate the degree of anisotropy can be related to the angle α between the absorption and fluorescing dipole by

$$P = \frac{2}{5}\left(\frac{3\cos^2(\alpha) - 1}{2}\right). \tag{2}$$

The anisotropy can range between 0.4 if the absorption and fluorescence dipoles point in the same direction and −0.2 if they are perpendicular. As can be seen in Fig. 2, the direction of the transition dipole for the ^1L_a state is parallel to the ^1B_a state and roughly perpendicular to the ^1B_b state, which is the same for pyrene and predicted by simple group theory arguments for a molecule with D_{2h} symmetry. The direction of the transition dipole remains relatively constant across the entire ^1L_a band. This indicates that the ^1L_b state, which is hidden by the large ^1L_a band, has a relatively weak transition from the ground state because the direction of its transition dipole must be orthogonal to the ^1L_a state. If the ^1L_b state had an appreciable transition strength relative to the strongly allowed ^1L_a transition, it would cause a noticeable change in the anisotropy. The observation that the ^1L_b transition is weak is in agreement with the simple perimeter model[16] and with detailed calculations[15] that predict the relative intensity of the ^1L_b transition to be 85 times smaller than that of the

^1L_a transition. It should be noted that the emission anisotropy, which is the solid curve continuing the dashed excitation anisotropy curve, has the same dipole direction as the ^1L_a. This is consistent with the fluorescence occurring from the ^1L_a state.

Even though the ^1L_b transition is essentially forbidden by electronic dipole selection rules, it can clearly be seen using MCD spectroscopy. MCD spectroscopy measures the difference, $\Delta\varepsilon=\varepsilon_R-\varepsilon_L$, of the extinction coefficients for right (ε_R) and left (ε_L) handed circularly polarized light caused by a magnetic field parallel to the light propagation direction. The common way of displaying MCD spectra is in magnetically induced molar ellipticity, normalized for unit magnetic field strength, against wave number or wavelength $[\theta]_M(\tilde{\nu})$. Three numbers, known as the A, B, and C terms, are needed to characterize the contribution of the ith electronic transition to the MCD spectrum.[17] The spectrum can be written as

$$[\theta]_M(\tilde{\nu}) = -\sum_i \left[A_i f_i(\tilde{\nu}) + \left(B_i + \frac{C_i}{k_B T} \right) g_i(\tilde{\nu}) \right], \tag{3}$$

where $g_i(\tilde{\nu})$ is the line shape function and $f_i(\tilde{\nu})$ is the derivative of the line shape for the ith transition. The C term is nonzero only if the ground state is degenerate and a nonzero A term requires a degenerate excited state. As is true for most aromatic compounds, the ground state is nondegenerate for all molecules studied in this paper. It should further be noted that group theory predictions rule out the degeneracy of an excited state unless a threefold axis of symmetry is present.[17]

The lack of degeneracy of both the ground and excited states means that the MCD spectra for the molecules used in this study depend primarily on B terms. The B term can be written as

$$B_i = \mathrm{Im}\left\{ \sum_{k\neq 0} \frac{m_{k0}}{E_k - E_0} \cdot \mu_{0i} \times \mu_{ik} + \sum_{k\neq i} \frac{m_{ik}}{E_k - E_i} \cdot \mu_{0i} \times \mu_{ki} \right\}. \tag{4}$$

Here, E_k is the energy of the kth excited state and m and μ are the matrix elements for the magnetic and electric dipole moments, respectively. The two infinite sums account for the Zeeman effect produced by the magnetic field, which causes mixing of the ground state and the final state with all other electronic states. In practice, the above expression can be simplified considerably because only a few important terms are left from the summations. For two states to effectively mix, they must be close in energy, which, due to the large energy separation between the ground and excited states, generally makes the second summation more important than the first. In addition, because of the cross-product dependence, the electric transition dipole moments should be close to perpendicular to one another. What makes MCD spectroscopy particularly powerful for separating overlapping absorption bands is that for two states produced by mixing the corresponding states in the absence of the magnetic field, their contributions to the B terms will be of equal magnitude, but opposite in sign.

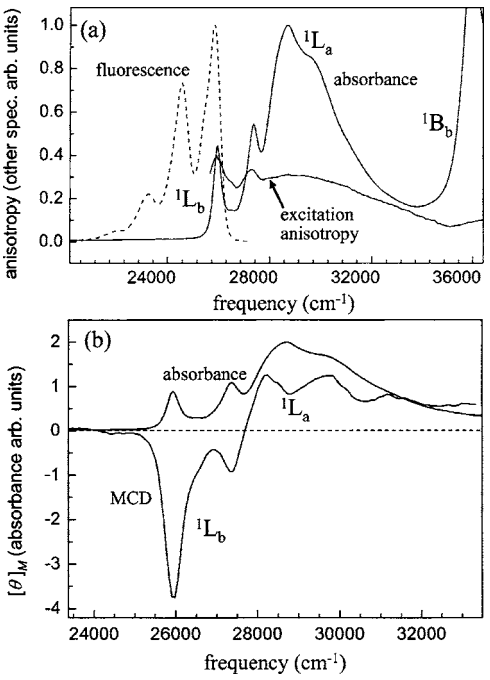

FIG. 3. (a) The absorption, fluorescence, and anisotropy spectra of PyOH in glycerol at 77 K. (b) The absorption and MCD spectra of PyOH in glycerol.

The theory for MCD spectroscopy for aromatic molecules has been well developed and provides a framework to make predictions concerning the signs of B terms for low-lying transitions based on substituent location and properties.[18–20] Pyrene and pyrene with various substitutions have been well studied.[21] In the terminology of Michl[20] and Moffitt,[22] pyrene is an odd-soft chromophore. Therefore, when substituted in a dominant position (positions 1, 3, 6, and 8 in Fig. 1), functional groups which inductively withdraw electron density (i.e., sulfate groups) will result in the sign sequence −, +, −, + for B terms in order of increasing energy for the first four transitions. Conversely, functional groups which donate electrons through resonance (i.e., hydroxyl groups) to a dominant position will have the opposite effect and give a +, −, +, − sign ordering to the MCD spectrum with increasing energy. By our definition of $[\theta]_M(\tilde{\nu})$, a negative B term will result in a positive MCD signal.

Figure 3 demonstrates this effect for pyrenol, which agrees with the results measured by Michl.[21] ^1L_b transition has been shown to be the lowest energy transition in the absorption spectrum.[21] In the MCD spectrum, the ^1L_b transition is negative in sign and the ^1L_a transition is positive. When the symmetry of the molecule is broken and the ^1L_b transition is allowed, there are two important points to take note that will be related to HPTS below. The first is that the ^1L_b transition has the same vibronic progression, with an approximately equal spacing of 1300 cm^{-1}, that occurs in the ^1L_a absorption and emission of $Py(SO_3)_4$, as well as other molecules discussed below. This progression can be seen in the absorption spectrum and is even more apparent in the fluorescence spectrum. The second important feature is that the ^1L_b transition dipole is close to but not along the long axis of the molecule. As in $Py(SO_3)_4$, the ^1L_a transition di-

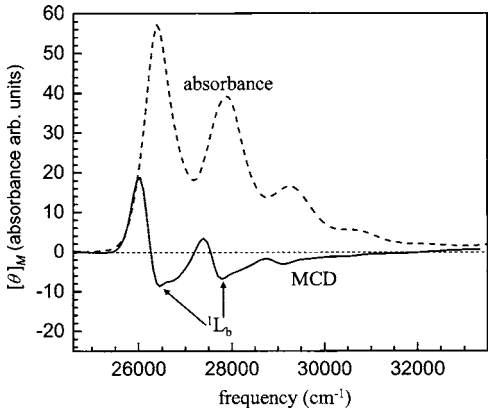

FIG. 4. Absorption and MCD spectra of $Py(SO_3)_4$ in glycerol. The absorption band shows only the ^1L_a transition, which is nearly degenerate with the ^1L_b transition, as can be determined through an analysis of the MCD spectrum.

pole is taken to be along the long axis with the ^1B_b transition dipole perpendicular to it along the short axis. From the anisotropy spectrum, the ^1L_b transition dipole direction can be estimated to be roughly 30° from the ^1L_a transition dipole and approximately 50° from the ^1B_b transition dipole. Within the uncertainty of the anisotropies of the overlapping bands, this is consistent with the ^1L_a and the ^1B_b transition dipoles perpendicular to, and with the ^1L_b transition dipole ~30° from, the long axis. Similar features are observed when comparing naphthalene to 2-naphthol.[23,24]

Figure 4 shows the MCD spectrum for $Py(SO_3)_4$ in the region of the ^1L_a band. This again follows the rules developed by Michl, and the lowest energy transition, the ^1L_a, is positive in sign. The ^1L_b and ^1L_a overlap and are opposite in sign with the ^1L_a transition, giving a positive contribution to the MCD spectrum. The line shapes of the MCD and absorption spectra match well in the rising edge, but it is impossible for us to strictly decompose the rest of the spectrum into a combination of ^1L_a or ^1L_b transitions because the two states overlap significantly and the spectrum may also have contributions from *A* terms. We can still estimate the energy of the ^1L_b transition to be approximately 26 500 cm^{-1} by the appearance of the first negative peak in the MCD spectrum. The negative peaks in the MCD spectrum also show the same characteristic vibronic structure as the ^1L_a absorption spectrum. The two states are very nearly degenerate, with the ^1L_a being slightly lower in energy. The near degeneracy combined with the orthogonality of the transition dipoles is the reason that $Py(SO_3)_4$ has a much more intense MCD signal than pyrenol.

The observation that the ^1L_a state is lower in energy is supported by the relatively short lifetime of $Py(SO_3)_4$ of 12.5 ns,[15] which indicates that the molecule fluoresces by an allowed transition. By comparison, pyrene has a very long excited state lifetime of 350 ns because the ^1L_b state is lower in energy than the ^1L_a state and the molecule must fluoresce from the ^1L_b state, which is a quasiforbidden transition. The relative positions of the ^1L_a and ^1L_b transitions of $Py(SO_3)_4$ and pyrene are compared in Fig. 5. Figure 5(a) shows the absorption spectra of $Py(SO_3)_4$ and pyrene and the MCD spectrum of $Py(SO_3)_4$, as discussed in connection with Fig. 4

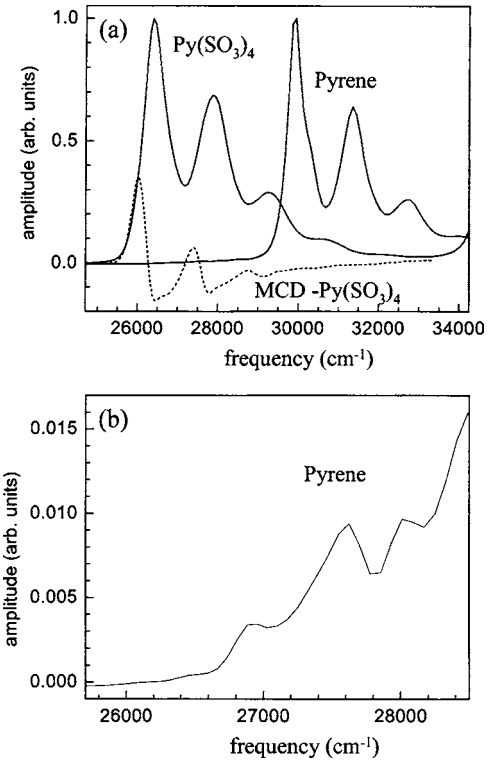

FIG. 5. (a)The absorption spectrum and MCD spectra of $Py(SO_3)_4$ and the absorption spectrum of pyrene in hexane. (b) A blowup of the raising low frequency edge of the very weak ^1L_b absorption of pyrene. Note the expanded frequency scale relative to (a). The ^1L_b state is approximately the same energy in both molecules, but the ^1L_a state is preferentially lowered in energy in $Py(SO_3)_4$ when compared to pyrene.

where it is shown that the ^1L_a state is only slightly lower in energy than the ^1L_b state. The strong features in the pyrene absorption spectrum correspond to transitions to the allowed ^1L_a state. Figure 5(b) shows a blowup (note expanded frequency scale) of the low frequency low amplitude rising edge of the pyrene absorption spectrum. These features arise from the absorption to the very weakly allowed ^1L_b state which is responsible for the long lived fluorescence. Comparing the pyrene absorption spectra to the $Py(SO_3)_4$ absorption and MCD spectra, it is seen that the ^1L_a transition of $Py(SO_3)_4$ is substantially lowered in energy by the electron-withdrawing groups along the long axis of the molecule (see Fig. 1), while the position of the ^1L_b band is only slightly affected. This has been documented for many aromatic molecules where the electron density is preferentially extended along one axis of the chromophore,[25] and can be explained by very primitive models such as the perimeter model.[16] In adding sulfate groups to the 1, 3, 6, and 8 positions of pyrene, electron density is inductively drawn to the ends of the long axis of the molecule and lowers the energy of an excited state with its transition dipole along the long axis.

Figure 6 shows the absorption, emission, and excitation anisotropy spectra for HPTS in glycerol. As in Fig. 2 showing spectra of $Py(SO_3)_4$, the anisotropy varies only slightly across the lowest energy absorption band. However, it can no longer be concluded that the ^1L_b transition is weak from this observation because breaking the molecular symmetry lifts the restriction that the ^1L_a and ^1L_b transition dipoles must be

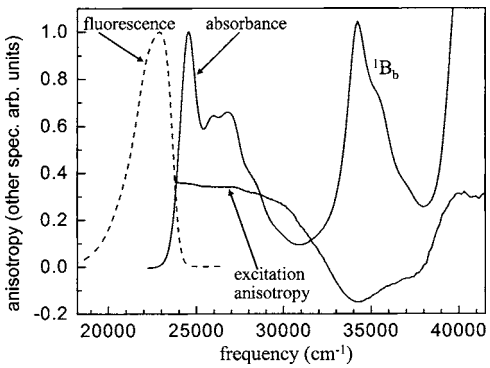

FIG. 6. Absorption, fluorescence, and excitation anisotropy spectra of HPTS in glycerol. The relatively constant excitation anisotropy across the lowest energy band indicates that the ^1L_a and ^1L_b dipoles are approximately parallel to each other.

perpendicular to one another. The ^1L_b transition can have substantial strength, but if its transition dipole is close to parallel to the ^1L_a transition dipole, then the nearly constant anisotropy of close to 0.4 would be expected. Van Gurp *et al.* made polarization studies of HPTS in a stretched polymer matrix,[26] but the possible existence of two transitions across this low energy band was not considered because of the seemingly constant anisotropy. There is no longer a clean vibronic progression of constant spacing in the absorption spectrum, as seen in Fig. 2. The washing out of the vibronic progression is consistent with the ^1L_b transition having an appreciable intensity.

The MCD and absorption spectra for HPTS (solid curves) appear in Fig. 7 along with the absorption spectrum of $Py(SO_3)_4$ (dashed curve) for comparison. HPTS has both inductive withdrawing and mesomeric donating substituents, but inductive effects have a much weaker influence than those of a strong π donor,[20] such as a hydroxyl group. A relative ordering of $-$, $+$, $-$, $+$ for the four lowest MCD transitions can then be expected.[20] The lowest energy transition shares the same sign as the third transition. This is also the situation for pyrenol. In Fig. 3(b), the alternation in sign $-$, $+$ for pyrenol can be seen for the first two transitions. The third transition [not shown in Fig. 3(b)] was observed to be negative. However, the sign does not reveal the identity of the transition. It is only by coincidence that the signs of the

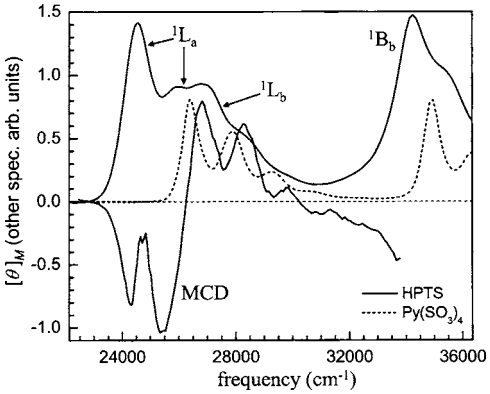

FIG. 7. The absorption and MCD spectra of HPTS in glycerol (solid curves). The absorption spectrum of $Py(SO_3)_4$ (dashed curve) is included for comparison.

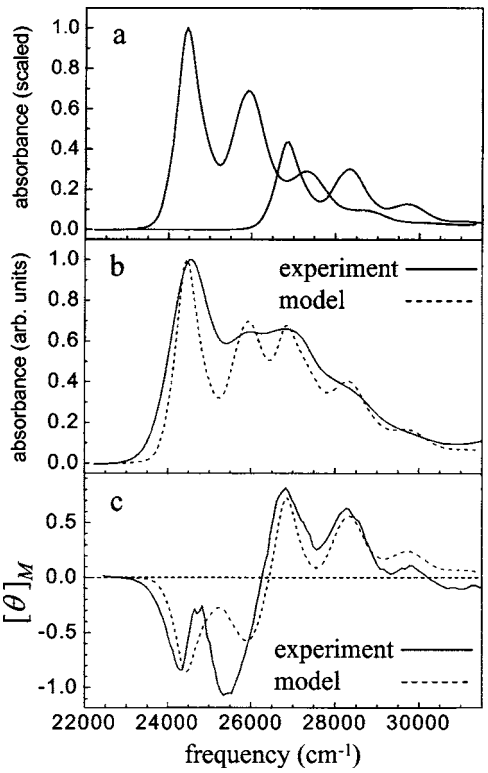

FIG. 8. (a) Shifted and scaled absorption spectra of $Py(SO_3)_4$. (b) The absorption spectrum of HPTS compared to a model consisting of the superposition of two shifted and scaled ^1L_a bands of $Py(SO_3)_4$ shown in (a). (c) The same two components in (a) with different scalings are used to represent the MCD spectrum.

^1L_a and ^1L_b transitions were the same for pyrenol and $Py(SO_3)_4$. What is immediately apparent is that the line shapes of both transitions in HPTS have the same vibronic progression seen in the ^1L_a transition for $Py(SO_3)_4$. The HPTS spectral features are much broader than those of $Py(SO_3)_4$, which is discussed in detail below. Nonetheless, the vibronic progression, particularly visible in the MCD spectrum, is clear.

Using the equivalence of the vibronic progressions in HPTS and $Py(SO_3)_4$, both the MCD and absorption spectrum can be reproduced fairly well by modeling them in terms of the ^1L_a absorption spectrum of $Py(SO_3)_4$ (see Fig. 2) to represent both the ^1L_a and ^1L_b absorption bands in HPTS. Figure 8 shows that the absorption spectrum of HPTS can be reproduced by blueshifting the ^1L_a band in $Py(SO_3)_4$ by 450 cm^{-1} and redshifting the same band by 1950 cm^{-1} to create the other component. Figure 8(a) shows the $Py(SO_3)_4$ shifted spectra scaled as they are used in Fig. 8(b). Figure 8(b) displays the HPTS absorption spectrum (solid curve) and the sum of the two spectra shown in Fig. 8(a) (dashed curve). The model fits the vibronic progression found in HPTS quite well, but substantial broadening of the HPTS spectral features (see below) relative to those of $Py(SO_3)_4$ is responsible for the reduced amplitude modulation of the experimental spectrum relative to the model spectrum. In spite of the widths of the HPTS spectral features, it is clear that the simple model reproduces the vibronic features. The method for properly simulating vibronic structure in MCD spectroscopy is significantly complex and discussed in detail

by Zgierski.[27,28] Here we only want to show that the relative positions of the ^1L_a and ^1L_b transitions, as shown in Fig. 8(a), are consistent with both the HPTS absorption and MCD spectra. To do this, the redshifted spectrum in Fig. 8(a) is inverted and added to the blue spectra. The spectra are scaled to match the amplitudes in the MCD spectrum. The result is shown in Fig. 8(c). The simple linear combination of absorption line shapes is not expected to reliably reproduce the MCD spectrum, although it is true that the MCD and absorption spectra of many well-separated strongly dipole allowed transitions are very similar. However, the simple model reproduces the negative and positive regions and the vibronic structure of the MCD spectrum relatively well.

It is interesting to compare how the ^1L_a and ^1L_b bands shift relative to one another when adding a hydroxyl functional group to pyrene versus the same substitution made to $Py(SO_3)_4$. When an alcohol is substituted at the 1 position of pyrene, both the ^1L_a and ^1L_b states are lowered in energy by a comparable amount (approximately 1500 and 1000 cm^{-1}, respectively). However, when an alcohol is substituted for a sulfonate group on $Py(SO_3)_4$, one state is lowered in energy more than either of the states for the pyrene to pyrenol case, but the other state actually increases in energy. It is unusual to witness a blueshift for a $\pi \rightarrow \pi^*$ transition when the π system of a chromophore is extended. The magnitudes and directions of the state shifts in going from $Py(SO_3)_4$ to HPTS are results of the accidental near degeneracy of the ^1L_a and ^1L_b states in $Py(SO_3)_4$. Because of the high symmetry of $Py(SO_3)_4$, the ^1L_a and ^1L_b states cannot directly couple even though they are closely spaced in energy. The addition of the hydroxyl shifts the two states to lower energy. However, once the symmetry is broken by the addition of the hydroxyl, the near degeneracy and strong coupling split the states. One state moves to lower energy and the other to higher energy relative to the energies they would have in the absence of coupling. As seen by the anisotropy spectrum in Fig. 6, adding the hydroxyl group to $Py(SO_3)_4$ to form HPTS causes such a large perturbation to the electronic structure that the ^1L_b transition dipole goes from being orthogonal to the ^1L_a dipole to being nearly parallel to it. In pyrene, the states are not close in energy initially. Adding the hydroxyl group lowers the energies of both states, but because of the substantial energy separation, no substantial mixing of the states occurs.

The sulfonate groups most likely intensify the state mixing in HPTS. The symmetry of the π system is broken because there is a significant overlap with an unhybridized p orbital on the oxygen atom. The presence of the three sulfonate groups in HPTS increases the overlap by inductively causing the withdrawal of electron density from the oxygen to the ring. This withdrawal of electron density results in a larger deviation from the local D_{2h} symmetry of the π network, which produces more effective state mixing in HPTS than pyrenol. ^1L_a-^1L_b mixing models have been suggested for naphthol[29,30] and recently for HPTS.[13] Because the states are strongly mixed in HPTS it may not be appropriate to refer to them by strict ^1L_a and ^1L_b definitions. Through level mixing, many of the empirical properties[16] used to describe typical ^1L_b states have been lost in HPTS, and instead both

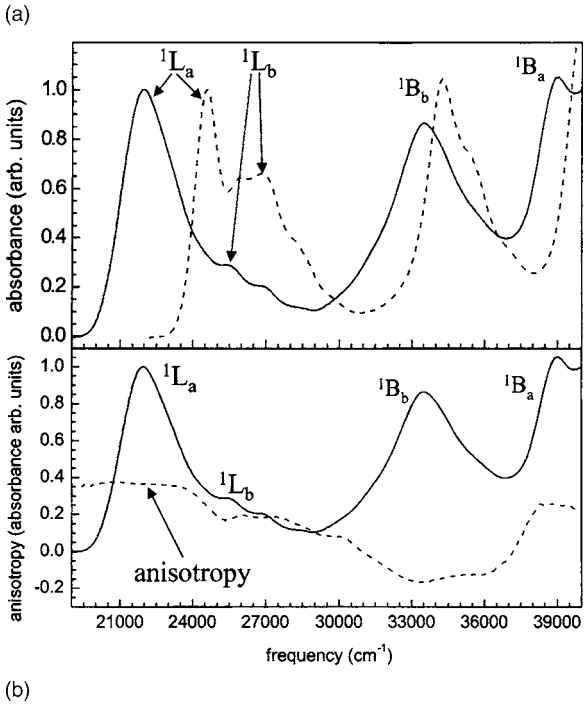

FIG. 9. (a) Comparison of protonated (dashed curve) and deprotonated (solid curve)absorption spectra of HPTS. (b) Absorption and anisotropy spectra of deprotonated HPTS in glycerol. Since the ^1L_a and ^1L_b dipoles no longer point in the same direction in the deprotonated state, they are resolvable in the excitation anisotropy spectrum by the drop in the anisotropy at $\sim$25 000 cm^{-1}.

transitions take the form of classic ^1L_a transitions. Our classification of the states is then limited to which has more ^1L_a or ^1L_b character.

There are several indications that the lowest energy state is the one most appropriate to be assigned to the ^1L_a state. As seen in Fig. 8(a), the model's basis spectra used to reproduce the experimental spectrum in Fig. 8(b), the oscillator strength for the lowest energy transition is roughly double that of the higher energy transition. The ^1L_a state is the more intense of the two transitions in the vast majority of aromatic compounds, and this is especially true for derivatives of pyrene.[21,31–34] Of more importance, in $Py(SO_3)_4$ the ^1L_a state is lower in energy than the ^1L_b state and, if the same effect applies to $Py(SO_3)_4$ that was observed for pyrene, adding a hydroxyl group to the ring will actually lower the energy slightly more for the ^1L_a state than for the ^1L_b state. It is generally observed that electron donating substituents in the 1 position of pyrene preferentially stabilize the ^1L_a state,[32] so this is a reasonable assumption.

HPTS was deprotonated in glycerol by adding a very small amount of sodium hydroxide. Figure 9(a) shows the deprotonated spectrum (solid curve) and the protonated spectrum (dashed curve). All four of the lowest energy transitions are redshifted in the deprotonated form. In deprotonating HPTS, the electron donating ability of the hydroxyl oxygen is increased and should preferentially lower the ^1L_a transition in energy relative to the ^1L_b transition, as observed in Fig. 9(a). Figure 9(b) shows the deprotonated spectrum and the excitation anisotropy spectrum for the deprotonated form. In contrast to Fig. 6, the deprotonated form displays a notice-

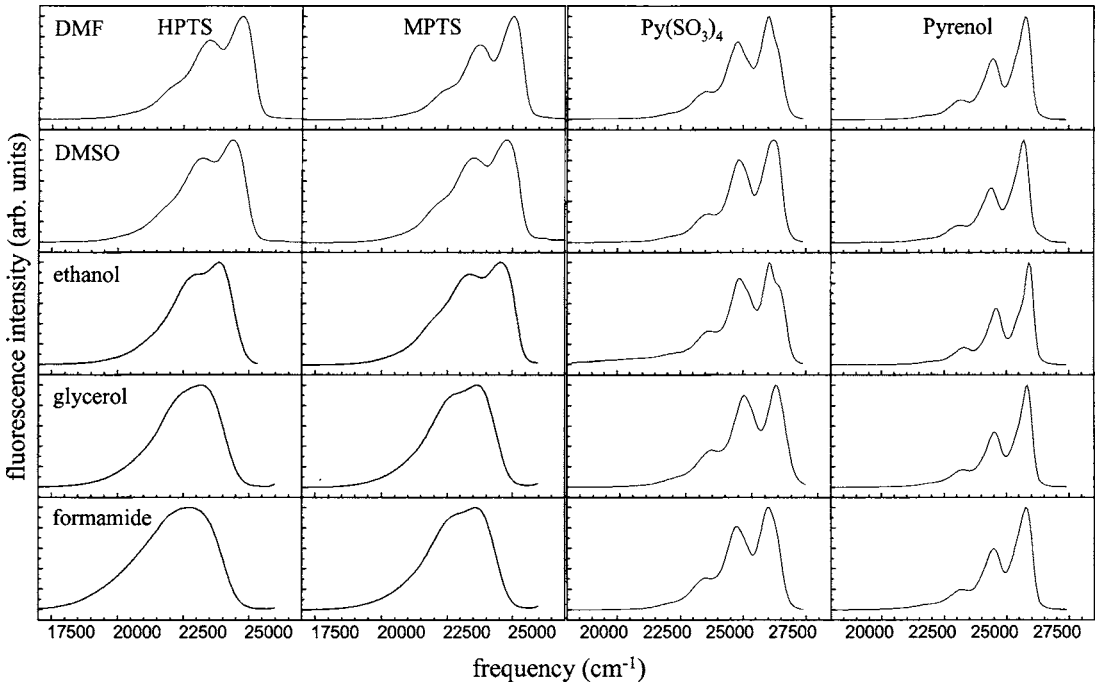

FIG. 10. Fluorescence spectra of HPTS, MPTS, $Py(SO_3)_4$, and pyrenol in different solvents. Going down the columns, the solvent has increased hydrogen bond donating ability. As the hydrogen bond donating ability of the solvent increases, the vibronic structures of HPTS and MPTS are washed out, but the vibronic structures of $Py(SO_3)_4$ and pyrenol are relatively unchanged.

able drop in anisotropy at the wavelength at which the ^1L_b absorption begins. The drop indicates that in the deprotonated state, the ^1L_a and ^1L_b transition dipoles no longer point in the same direction, but are separated by $\sim 35°$. The angle is calculated from the excitation anisotropy spectrum. The angle between the transition dipoles suggests less mixing of the states. The result is decreased intensity borrowed from the strongly allowed ^1L_a transition, which reduces the oscillator strength of the ^1L_b transition in the deprotonated form relative to the protonated form. The increase in π donation from the hydroxyl oxygen to the ring in the deprotonated form produces a significant broadening of the vibronic structure for all electronic transitions. The increased broadening is a general consequence of increased electron donation to the aromatic ring and will be discussed further in the next section.

The analysis of the absorption, fluorescence, excitation anisotropy, and MCD spectra of the various compounds demonstrates that the lowest electronic state of protonated HPTS is the ^1L_a state followed by the ^1L_b state. However, these states are heavily mixed, and the significant oscillator strength of the ^1L_b state comes from this mixing. Deprotonation shifts both the ^1L_a state and the ^1L_b state to lower energy with a larger shift for the ^1L_a. Thus the state ordering is unchanged. The shift to lower energy of the states in the deprotonated form is caused by the donation of electron density to the π system from the hydroxyl oxygen. When HPTS is electronically excited but prior to full deprotonation, electron density is also transferred to the π system. Because full deprotonation preserves the state ordering, there is nothing to suggest that there is a change in the state ordering[15] upon electronic excitation. In the next section it will be shown that the solvent dependent changes in line broadening can also be accounted for without a mechanism that involves changes in state ordering or substantial changes in the energy separations of the states.

B. Mechanism for solvent dependent line shapes: A Brownian oscillator model

The fluorescence line shape of HPTS is heavily dependent on the nature of solvent, a fact that has been commented on by several authors.[13–15] For solvents that have only weak hydrogen bonding interactions, the fluorescence spectrum of HPTS shows a vibronic progression with an approximate spacing of 1300 cm^{-1}. This vibronic structure is substantially reduced or disappears in solvents that serve as appreciable hydrogen bond donors, such as ethanol. Figure 10 shows the solvent dependence of the fluorescence spectra of four molecules in five solvents. The four molecules are HPTS, the methoxy derivative of HPTS that has been referred to in another study as MPTS (Ref. 13) (see Fig. 1), $Py(SO_3)_4$, and pyrenol. The solvents are dimethyl formamide, dimethyl sulfoxide, ethanol, glycerol, and formamide. These solvents, from top to bottom in Fig. 10, are in order of increasing ability to donate a hydrogen bond. As seen in Fig. 10, going from top to bottom, both HPTS and MPTS show decreasing and finally no vibronic structure while both $Py(SO_3)_4$ and pyrenol display little or no change in their vibronic structure. Similar observations have been reported previously.[13–15]

The changes in vibronic structure with solvent seen in HPTS are quite common in charge-transfer complexes.[35,36] The changes in the fluorescence spectrum with solvent have led to suggested mechanisms involving different charge distributions in the HPTS[13,15] or charge-transfer (CT) and locally excited (LE) states, which are dictated by the solvent.

In the specific model suggested by Tran-Thi, the LE state corresponds to the ^1L_b state and the CT state is the ^1L_a state, and inversion of the energies of the two states is controlled by a solvent reorganization in the excited state. The mixed ^1L_a-^1L_b version of the state inversion model is equivalent to an avoided curve crossing between the ^1L_a and ^1L_b states that results in the lowest energy state adopting more ^1L_a (or charge transfer) character in polar solvents.

State inversion is in conflict with the detailed assignment given above the ^1L_a state being the lowest energy excited state in both the protonated and deprotonated forms of HPTS. In this section an explanation that accounts for the changes in the fluorescence line shape with solvent that does not depend on the requirement that there is a state inversion is presented. It will be shown that a simple Brownian oscillator model of the dephasing of vibronic transitions can account for the observed trends in terms of the strength of the coupling between the electronic states and the solvent. The Brownian oscillator model used here has been successful in reproducing vibronic spectra in other systems.[37–40] Mukamel and Yan gave an excellent review of this topic.[41]

Because MPTS and HPTS differ only by the inability of MPTS to donate a hydrogen bond to the solvent, it can be seen from Fig. 10 that the hydrogen bond accepting ability of the solvent has a minor effect on the fluorescence spectra of HPTS. The line shape of the fluorescence spectra is, however, heavily dependent on the hydrogen bond donating ability of the solvent. There is also most likely a weak dependence on the polarity of the solvent, but its effect is relatively small when compared to hydrogen bond donation. The small role played by polarity can be seen by comparing the Kamlet-Taft (KT) parameters for the various solvents,[42] which have been extensively used to describe solvatochromism in a wide range of photoacids,[15,17,43–47] but the specific importance of hydrogen bonding can be immediately illustrated by comparing dimethylformamide (DMF) to formamide. Both solvents are similar in structure and have a relatively high polarity, but formamide, because of its ability to donate hydrogen bonds, dramatically broadens the HPTS and MPTS fluorescence spectra while DMF does not.

There are a number of hydrogen bond accepting sites on HPTS, making it possible for the hydrogen bond donation ability of the solvent to have a dramatic effect on the fluorescence spectrum. In principle, HPTS has two different sites that might serve as hydrogen bond acceptors. The lone pair electrons of the alcohol functional group could accept hydrogen bonds from the solvent. Since they have a significant overlap with the π system of the aromatic ring, this interaction could potentially influence the charge distribution and therefore the electronic states. Hydrogen bond donation to the hydroxyl oxygen is most likely not important in HPTS because the fluorescence spectrum of pyrenol does not demonstrate significant broadening in strong hydrogen bonding environments (see Fig. 10). Although pyrenol and many pyrenol derivatives have been shown to form strong hydrogen bonds with hydrogen bonding acceptors, they tend to not accept hydrogen bonds.[47] Therefore, the most important hydrogen bonding interactions for determining the fluorescence line shape of HPTS are with the three sulfonate groups.

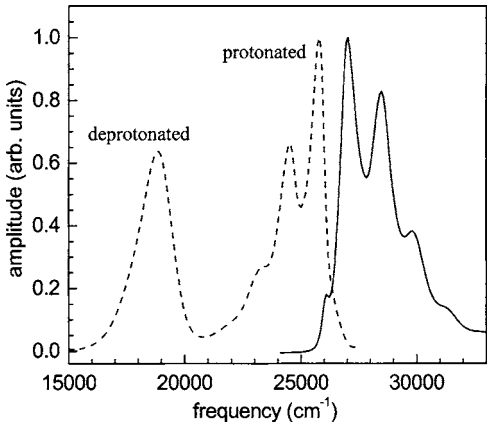

FIG. 11. Absorption (solid curve) and fluorescence (dashed curve) spectra of APTS. The fluorescence spectrum takes in a 90% sulfuric acid solution. The protonated and deprotonated states are seen at ~26 000 and ~21 000 cm^{-1}, respectively.

However, hydrogen bond donation to the sulfonates alone cannot be responsible for the spectral broadening because $Py(SO_3)_4$ does not show the broadening in the same solvents (see Fig. 10). Barrash-Shiftan *et al.* have made a similar comment relating to solvatochromism studies.[14]

Further insight can be obtained by comparing HPTS to the related photoacid APTS (see Fig. 1). APTS is the amine-substituted relative of HPTS. APTS is a much stronger photoacid, with an excited state *pKa* comparable to the strongest mineral acids. The protonated form of APTS retains a well-defined vibronic progression in its fluorescence spectrum even in an extremely strong hydrogen bonding environment, such as a 90% sulfuric acid solution (see Fig. 11). The electron lone pairs of the hydroxyl oxygen on HPTS are coupled to the π system of the aromatic ring structure. The absence of unpaired electrons on the amine in the protonated form of APTS inhibits substantial coupling between the π system and the amine substituent. This difference between HPTS and APTS is responsible for the fact that the lowest $\pi \rightarrow \pi^*$ transition frequency is significantly higher in energy in APTS than in HPTS.

The sulfonate groups primarily act to inductively withdraw electron density from the pyrene ring, but they contribute very little orbital overlap to the π system. The lack of π orbital overlap in HPTS is evidenced by the small resonance Hammett substituent constant[48] (σ_R) of 0.07. The lack of π orbital overlap between sulfonate groups and the π system of the aromatic system to which they are substituents has been discussed in explaining why cyanonaphthols are much stronger photoacids than naphthol sulfonates.[49]

The sulfonate groups do play an important role in the photoacidity of HPTS by working in a cooperative manner with the alcohol to redistribute electron density from the hydroxyl oxygen to the ring in the excited state. By accepting hydrogen bonds with the surrounding solvent, the sulfonate groups become stronger electron-withdrawing substituents and more effectively pull charge density into the aromatic ring from the hydroxyl group. Evidence for the dependence of the inductive strength of sulfonate groups on hydrogen bonding is suggested by the inductive Hammett substituent

constant (σ_I). For $-SO_2OR$ the inductive strength is double (0.44) that of $-SO_3^-$(0.2). For a hydrogen bonded sulfonate group, $-SO_3^- - H - O$, the hydrogen bonded group will have an influence less than a covalently bonded R group but greater than no group at all. Therefore, σ_I for the hydrogen bonded sulfonate should be between 0.44 and 0.2.

The importance of hydrogen bonding to the sulfonate group is consistent with pyrenol, naphthol,[43] and even cyanonaphthols,[44,45] which do not demonstrate a strong dependence of their fluorescence spectra on hydrogen bond donating ability of the solvent. As the strength of the hydrogen bond donating ability to the sulfonate groups on HPTS is increased, there is an increased redistribution of electron density into the aromatic ring from the hydroxyl group. Thus, hydrogen bonding to the sulfonates provides a mechanism for strongly coupling the electronic transition of HPTS to the solvent. The increased coupling of the electronic states as the solvent's hydrogen bond donating ability is increased and is demonstrated by the change in both the absorption frequency[14] and the emission frequency (see Fig. 10). At room temperature, rapid structural fluctuations of the solvent which are coupled to an electronic transition produce dephasing of the electronic transition, which manifests itself as line broadening. As the coupling to the solvent grows, the dephasing will increase. Here we propose that structural fluctuations of the solvent produce fluctuations in the hydrogen bonding to the sulfonates, which in turn produce fluctuations in the π electron distribution, therefore, fluctuations in the electronic transition energy. The extent of these fluctuations, and therefore the dephasing and associated line broadening, grows as the hydrogen bond donating ability of the solvent increases. Then the key to the changes in line shapes of HPTS and MPTS but not of pyrenol or $Py(SO_3)_4$ seen in Fig. 10 is the increased coupling of solvent dynamics to the electronic transition with increased hydrogen bond donation. A simple Brownian oscillator model of electronic vibronic transition-solvent coupling can illustrate the influence of increased coupling to solvent fluctuations.

Mukamel has used a cumulant expansion truncated at second order to describe both the linear and nonlinear responses of a system to the application of one or more radiation fields.[37] In this approach, which is very briefly outlined here to introduce the necessary parameters and method of calculation, the experimental observables are obtained from the frequency-frequency correlation function (FFCF). The FFCF depends on the physical nature of the system. In terms of the response function methodology, the fluorescence spectrum is expressed as

$$I_f(\omega) = \frac{1}{\pi} \mathrm{Re}\left[\int_0^\infty \exp(i\omega t - g^*(t))dt\right], \tag{5}$$

where $g(t)$ is called the line shape function. The line shape function is related to the time dependent FFCF $\langle\omega(t)\omega(0)\rangle$ by[37]

$$g(t) = \int_0^t \int_0^\tau \langle\omega(\tau')\omega(0)\rangle d\tau' d\tau''. \tag{6}$$

Therefore, once the FFCF is specified, the fluorescence line shape can be calculated. Here the influence of the solvent will be brought in by the coupling of the vibronic transitions to a Brownian oscillator model of the solvent. Following Mukamel the calculation can be cast in terms of classical mechanics.[37]

For pyrene and pyrene derivatives studied in this paper, both absorption and fluorescence spectra show a well-defined vibronic progression that has an almost constant spacing. This phenomenon was commented on in the 1930s when it was noticed in a wide range of pyrene compounds.[34] The vibronic modes of the ^1L_a transition in pyrene have been studied by several high-resolution spectroscopic methods.[50,51] The results of these studies reveal a complex structure composed primarily of relatively weak intensity b_{3g} modes centered around a strongly allowed a_g mode. The a_g mode also induces vibrational coupling to the nearby ^1L_b state. This strongly allowed a_g mode is a symmetric C–C ring vibration, and its specific nature is most likely one which lengthens and shortens the bonds in phase, which is similar to the bond length changes that occur on excitation.[25] Because the a_g mode dominates the vibronic progression, it is the only one included explicitly in the model. In a low temperature system where multiple modes can be observed, more than one mode can be treated as demonstrated for anthracene at low temperature by Shan *et al.*[40] However, for the molecules studied here at higher temperatures the distribution of modes can be represented by a convolution of the single mode explicitly treated with a Gaussian distribution function. The Gaussian distribution function reflects the set of low frequency modes that are not resolved in the spectrum but contribute to the width of each of the observed vibronic lines. The set of low frequency modes is essentially independent of the solvent. As discussed below, the width of the Gaussian is kept fixed independent of the solvent. This approach is mathematically equivalent to representing the FFCF in terms of a time dependent contribution $C(t)$ that arises from coupling of the molecular states to the solvent and a time independent contribution Δ that reflects the line broadening associated with the unresolved low frequency modes,

$$\langle\omega(t)\omega(0)\rangle = C(t) + \Delta. \tag{7}$$

In this form, the effect of Δ is analogous to inhomogeneous broadening.

The specific nature of the vibration that gives rise to the vibronic progression is unimportant as long as it can be reasonably approximated as a nuclear motion in a harmonic well. The molecule is modeled as a pair of electronic states that are coupled to the nuclear motions of the molecule. The excited state is displaced relative to the ground state. Here we will treat a single internal molecular mode called the primary mode. The primary mode is coupled to a set of bath (solvent) modes. The bath modes are not treated explicitly. Rather a Brownian oscillator accounts for the interaction between this primary mode and a collection of linearly coupled

bath oscillators. It is shown by Mukamel that it is possible to simplify this problem considerably by mapping it onto a single classical harmonic oscillator and include the quantum mechanical aspects through a semiclassical correction, which is exactly equivalent to a full quantum mechanical treatment in the harmonic oscillator case.[37] The method treats the bath modes through a generalized damping term.

The Hamiltonian contains terms for a two electronic state system consisting of two offset harmonic potentials. The minimum of the ground state energy is taken to be zero. Therefore, there is no electronic term in the ground state Hamiltonian H_g. The energy of the electronic excited state is E_{eg}, which appears as the electronic term in the excited state Hamiltonian H_e. q and p are the position and momentum of the primary vibrational mode, respectively, m is the reduced mass, ω is the oscillator frequency, and d is the offset of the minima of the two harmonic wells of the two electronic states,

$$H_g(p,q) = \frac{p^2}{2m} + \frac{1}{2}m\omega^2 q^2, \tag{8}$$

$$H_e(p,q) = E_{eg} + \frac{p^2}{2m} + \frac{1}{2}m\omega^2(q+d)^2. \tag{9}$$

The transition energy is

$$\Delta E_{eg} = E_{eg} + \tfrac{1}{2}m\omega^2 d^2 + U, \tag{10}$$

where

$$U = m\omega^2 dq. \tag{11}$$

U contains the nuclear coordinate (q) of the primary mode, which is coupled to the bath modes. Through the coupling to the bath modes, q fluctuates causing the transition energy to fluctuate. The fluctuation in the transition energy results in dephasing of the electronic transition and is responsible for the dynamical broadening of the vibronic transitions [$C(t)$ in Eq. (7)].

In the model, the nuclear coordinate of the primary mode, q, is subject to a stochastic force $f(t)$, which is equivalent to coupling to a set of quantum mechanical bath modes. The fluctuations of q can be obtained using the Langevin equation[52,53]

$$\ddot{q}(t) + \gamma\dot{q}(t) + \omega^2 q(t) = \frac{f(t)}{m}, \tag{12}$$

where γ is the damping.

For two displaced harmonic potentials, the energy difference between the ground and excited states depends linearly on the primary mode nuclear coordinate q [see Eq. (11)], and the time dependent portion of the frequency-frequency correlation function for the vibronic transitions can be shown to be[37]

$$C(t) = \left(\frac{m\omega^2 d}{\hbar}\right)^2 \langle q(t)q(0)\rangle. \tag{13}$$

The classical position-position correlation function for the model under consideration can be obtained exactly, but it is then necessary to transform this classical correlation function into its quantum mechanical counterpart, which can be accomplished in several ways, which give the same result.[37] Using the resulting quantum position-position correlation function, the FFCF is obtained. It is convenient to express the FFCF in terms of its real and imaginary components, and the two parts are related through the fluctuation-dissipation theorem in the frequency domain,[54]

$$C(t) = C(t) + iC''(t), \tag{14}$$

$$\tilde{C}'(\omega) = \coth\left(\frac{\hbar\omega}{2k_B T}\right)\tilde{C}''(\omega), \tag{15}$$

where the tilde indicates Fourier transformation. Here only $C''(t)$ is written out because its functional form is compact,

$$C''(t) = -\frac{\hbar}{2m\zeta}\exp(-\gamma|t|)\sin(\zeta t), \tag{16}$$

where

$$\zeta^2 = \omega^2 - \gamma^2/4. \tag{17}$$

$C'(t)$ is obtained by Fourier transforming $C''(t)$, employing Eq. (15), and then back Fourier transforming. The analytic solution is given in Chap. 8 of *Principles of Nonlinear Optical Spectroscopy* by Mukamel.[37] The full solution [Eq. (14)] gives a series of peaks that have widths and magnitudes determined by the input parameters.

The model depends on relatively few parameters, and they can be readily assigned from the fluorescence spectrum. The displacement of the harmonic wells between the ground and excited states, d, controls Frank-Condon factors in the electronic transition, which translates into the relative amplitudes of peaks in the vibronic progression. The vibrational frequency ω is determined by the vibronic spacing of the spectrum. The damping parameter γ describes the interaction of the oscillation with the surroundings. Increasing vibrational damping has the effect of broadening each vibronic line. As the lines become broader, the vibronic structure washes out. In the current application, γ reflects the interaction between the solvent and chromophore. Stronger coupling to the solvent results in increased linewidth. As given in Eq. (7), in addition to the time dependent contribution to the FFCF, there is the static contribution Δ, which is the broadening of the observed vibronic transitions by the unresolved distribution of low frequency modes.

Figures 8(a) and 8(b) illustrate how the absorption bands of both the ^1L_a and ^1L_b states in HPTS can be created from the ^1L_a line shape of $Py(SO_3)_4$. By assuming that the basic line shapes of the ^1L_a transition in $Py(SO_3)_4$ and HPTS are the same, we can model the fluorescence spectrum for HPTS. Figure 12 shows the experimental fluorescence spectrum for $Py(SO_3)_4$ (solid curve) and the fit (dashed curve) using the Brownian oscillator model outlined above with $\omega = 1250\ \text{cm}^{-1}$, $\gamma = 220\ \text{cm}^{-1}$, $\Delta = 1.8\times10^9\ \text{s}^{-2}$, and $\delta = 1.4$ at a temperature of 300 K. δ is the reduced displacement parameter given by $\delta = (m\omega/\hbar)^{1/2}d$.

The parameters are relatively independent. ω is largely determined by the spacing of the peaks in the progression. γ is determined by the linewidths and their change with the

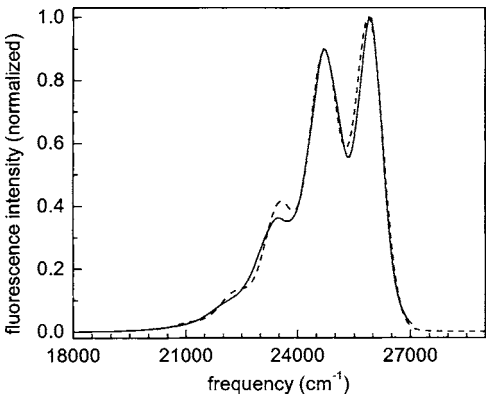

FIG. 12. Single Brownian oscillator model fit (dashed curve) to the fluorescence spectrum of $Py(SO_3)_4$ (solid curve) with $\gamma=220\ cm^{-1}$, $\omega=1250\ cm^{-1}$, $\delta=1.4$, and $\Delta=1.8\times10^9\ s^{-2}$.

quantum number n of the vibronic progression. δ is largely determined by the progression of peak amplitudes. The inhomogeneous parameter, which accounts for the unresolved low frequency modes, Δ is readily obtained because it is independent of n but the width of the vibronic lines in the progression increases as n increases. All of the parameters play off against each other to some extent, but there is only a very small range of parameters that give a reasonable fit to the spectrum. Considering the simplicity of the Brownian oscillator model, the agreement is quite good. The damping parameter can then be varied to reflect the coupling strength of the chromophore with the various solvents.

Figure 13 shows calculated fluorescence spectra which

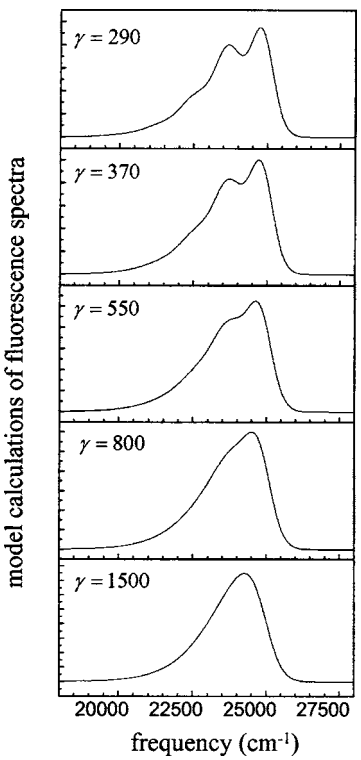

FIG. 13. Calculated curves using the Browning oscillator model. Only the parameter γ, which reflects the strength of coupling of the electronic transition to the solvent, is varied. The other parameters are those obtained from the fit to the fluorescence spectrum of $Py(SO_3)_4$ (see Fig. 12). As the coupling strength increases, the vibronic structure is washed out.

are rough models of the fluorescence spectra of HPTS and MPTS in various solvents, as shown in the first two columns of Fig. 10. The calculated curves are not fits to the data but rather are intended to show the trends as γ, which reflects the coupling strength of the vibronic transition to the solvent, is increased. All of the parameters obtained from the fit of the $Py(SO_3)_4$ spectrum are fixed at their $Py(SO_3)_4$ values, with the exception of γ. Going from top to bottom, there is gradual loss of vibronic structure as γ is increased. The calculated trends clearly reproduce the trends observed in Fig. 10.

The model calculations demonstrate that the solvent dependence of the vibronic structure can be accounted for by the difference in the strength of coupling between the electronic states and the solvent. In the first part of this section it was argued that an increase in hydrogen bond donation from the solvent to the sulfonate groups tracked the changes observed in the solvent dependence of the vibronic structure of HPTS and MTPS. The dynamic electronic dephasing that produces the line broadening and the washing out of the vibronic structure comes from structural fluctuations of the solvent hydrogen bonds to the sulfonates. Stronger hydrogen bonds (increased coupling) transfer the solvent fluctuations into greater electronic dephasing and increased line broadening.

IV. CONCLUDING REMARKS

MCD and polarization spectroscopy were used to separate the two lowest states of HPTS in both the protonated and deprotonated forms. The results demonstrate that the ^1L_a-^1L_b are states strongly mixed, and the lowest state in both the protonated and deprotonated forms has a primarily ^1L_a character. In the protonated form of HPTS, transitions from the ground state to both states have nearly parallel transition dipoles and are relatively close in energy, which allows the ^1L_b transition to gain oscillator strength from intensity borrowing (about half of the strongly allowed ^1L_a transition). The strength of the transition to the ^1L_b state in the protonated form is in contrast to the deprotonated molecule, where the two transition dipoles no longer point in the same direction and the ^1L_b transition is much weaker, which is the case for most pyrene derivatives.

The assignment of the lowest excited state of both protonated and deprotonated HPTS to the same electronic state is clearly in conflict with either direct or avoided curve crossing associated with deprotonation.[15] Using a Brownian oscillator model, calculations showed that it is possible to explain the solvent dependence of the vibronic structure of HPTS by solvent induced electronic dephasing. It is not necessary to invoke a solvent dependent electronic excited state crossing to explicate the solvent dependence of the vibronic structure (see Fig. 10 and 13). The extent of the dephasing is largely dictated by the hydrogen bond donation ability of the solvent. The most probable interaction leading to increased dephasing is hydrogen bonding to the three sulfonate groups, which increases their ability to inductively pull electron density into the aromatic ring from the hydroxyl oxygen. Solvent fluctuations modulate the hydrogen bonding to the sul-

fonate groups and thereby produce fluctuation in the π system electron distribution with associated electronic dephasing.

ACKNOWLEDGMENTS

This work was supported by the Department of Energy (DE-FG03-84ER13251). One of the authors (D.B.S.) thanks the National Science Foundation for a NSF Fellowship. The authors would also like to thank Professor Edward I. Solomon for the use of his MCD apparatus and student time supported under NSF Grant No. MCB-0342807.

[1] T. Förster, Z. Elektrochem. **54**, 531 (1950).
[2] A. Weller, Z. Phys. Chem. (Munich) **17**, 224 (1958).
[3] T. Förster and S. Volker, Chem. Phys. Lett. **34**, 1 (1975).
[4] D. Huppert, Chem. Phys. Lett. **126**, 88 (1986).
[5] E. Pines, D. Huppert, and N. Agmon, J. Chem. Phys. **88**, 5629 (1988).
[6] K. Ando and J. T. Hynes, J. Phys. Chem. B **101**, 10464 (1997).
[7] N. Agmon, J. Phys. Chem. A **109**, 13 (2005).
[8] T. Elsaesser and H. J. Bakker, *Ultrafast Hydrogen Bonding Dynamics and Proton Transfer Processes in the Condensed Phase* (Kluwer, Dordrecht, 2002).
[9] J. T. Hynes, T.-H. Tran-Thi, and G. Granucci, J. Photochem. Photobiol., A **154**, 3 (2002).
[10] T.-H. Tran-Thi, T. Gustavsson, C. Prayer, S. Pommeret, and J. T. Hynes, Chem. Phys. Lett. **329**, 421 (2000).
[11] R. Gepshtein, P. Leiderman, L. Genosar, and D. Huppert, J. Phys. Chem. A **109**, 9674 (2005).
[12] P. Leiderman, L. Genosar, and D. Huppert, J. Phys. Chem. A **109**, 5965 (2005).
[13] O. F. Mohammed, J. Dreyer, B.-Z. Magnes, E. Pines, and E. T. J. Nibbering, ChemPhysChem **6**, 625 (2005).
[14] N. Barrash-Shiftan, B. Brauer, and E. Pines, J. Phys. Org. Chem. **11**, 734 (1998).
[15] T. H. Tran-Thi, C. Prayer, P. Millie, P. Uznanski, and J. T. Hynes, J. Phys. Chem. A **106**, 2244 (2002).
[16] J. R. Platt, J. Chem. Phys. **17**, 484 (1949).
[17] M. Klessinger and J. Michl, *Excited States and Photochemistry of Organic Molecules* (VCH, New York, 1994).
[18] J. Michl, J. Am. Chem. Soc. **100**, 6801 (1978).
[19] J. Michl, J. Am. Chem. Soc. **100**, 6812 (1978).
[20] J. Michl, J. Am. Chem. Soc. **100**, 6819 (1978).
[21] J. Michl, J. Am. Chem. Soc. **100**, 6872 (1978).
[22] W. Moffitt, J. Chem. Phys. **22**, 320 (1954).
[23] K. R. Popov and L. V. Smirnov, Opt. Spektrosk. **28**, 1134 (1970).
[24] K. Nishimoto and R. Fujishiro, J. Chem. Phys. **36**, 3494 (1962).
[25] J. N. Murrell, *The Theory of the Electronic Spectra of Organic Molecules* (Wiley, New York, 1964).
[26] M. Van Gurp, T. Van Heijnsbergen, G. Van Ginkel, and Y. K. Levine, J. Chem. Phys. **90**, 4103 (1989).
[27] M. Z. Zgierski, J. Chem. Phys. **85**, 109 (1986).
[28] M. Z. Zgierski, J. Chem. Phys. **83**, 2170 (1985).
[29] R. Knochenmuss, P. L. Muino, and C. Wickleder, J. Chem. Phys. **100**, 11218 (1996).
[30] R. Knochenmuss and S. Leutwyler, J. Chem. Phys. **91**, 1989 (1989).
[31] G. Forester and J. Wagner, Z. Phys. Chem. Abt. B **37**, 353 (1937).
[32] V. Baliah and M. K. Pillay, Indian J. Chem. **9**, 815 (1971).
[33] R. S. Becker, I. S. Singh, and E. A. Jackson, J. Chem. Phys. **38**, 2144 (1963).
[34] C. Sannie and V. Poremski, Bull. Soc. Chim. **3**, 1139 (1936).
[35] S. G. Schulman, *Fluorescence and Phosphorescence Spectroscopy: Physicochemical Principles and Practice* (Pergamon, New York, 1977).
[36] R. Foster, *Organic Charge-Transfer Complexes* (Acadenic, London, 1969).
[37] S. Mukamel, *Principles of Nonlinear Optical Spectroscopy* (Oxford University Press, New York, 1995).
[38] L. D. Book and N. F. Scherer, J. Chem. Phys. **111**, 792 (1999).
[39] E. T. J. Nibbering, D. A. Wiersma, and K. Duppen, Chem. Phys. **183**, 167 (1994).
[40] K. Shan, Y. Jing, and S. Mukamel, J. Chem. Phys. **87**, 2021 (1987).
[41] S. Mukamel and Y. J. Yan, J. Chem. Phys. **89**, 5160 (1988).
[42] Y. Marcus, M. J. Kamlet, and R. W. Taft, J. Phys. Chem. **92**, 3613 (1988).
[43] K. M. Solntsev, D. Huppert, and N. Agmon, J. Phys. Chem. A **102**, 9599 (1998).
[44] K. M. Solntsev, D. Huppert, L. M. Tolbert, and N. Agmon, J. Am. Chem. Soc. **120**, 7981 (1998).
[45] K. M. Solntsev, D. Huppert, and N. Agmon, J. Phys. Chem. A **103**, 6984 (1999).
[46] N. Mataga and T. Kubota, *Molecular Interactions and Electronic Spectra* (Dekker, New York, 1970).
[47] Z. Rappoprot, *The Chemistry of Phenols* (Wiley, New York, 2003).
[48] N. Isaacs, *Physical Organic Chemistry*, 2nd ed., (Wiley, New York, 1995).
[49] L. M. Tolbert and J. E. Haubrich, J. Am. Chem. Soc. **112**, 8163 (1990).
[50] N. Ohta, H. Baba, and G. Marconi, Chem. Phys. Lett. **133**, 222 (1987).
[51] G. Rouille, S. Krasnokutski, F. Huisken, T. Henning, O. Sukhorukov, and A. Staica, J. Chem. Phys. **120**, 6028 (2004).
[52] M. C. Wang and G. E. Uhlenbeck, Rev. Mod. Phys. **17**, 323 (1945).
[53] S. Chandrasekhar, Rev. Mod. Phys. **15**, 1 (1943).
[54] R. Zwanzig, *Nonequilibrium Statistical Mechanics* (Oxford University Press, New York, 2001).